Accelerated Publications

Structure of 4-Chlorobenzoyl Coenzyme A Dehalogenase Determined to 1.8 Å Resolution: An Enzyme Catalyst Generated via Adaptive Mutation[†,‡]

Matthew M. Benning,[§] Kimberly L. Taylor,[||] Rui-Qin Liu,[||] Guang Yang,[||] Hong Xiang,[||] Gary Wesenberg,[§] Debra Dunaway-Mariano,*[,||] and Hazel M. Holden*[,§]

Department of Biochemistry and Institute for Enzyme Research, University of Wisconsin, 1710 University Avenue, Madison, Wisconsin 53705, and Department of Chemistry and Biochemistry, University of Maryland, College Park, Maryland 20742

Received April 1, 1996; Revised Manuscript Received April 29, 1996[⊗]

ABSTRACT: Here we describe the three-dimensional structure of 4-chlorobenzoyl-CoA dehalogenase from *Pseudomonas* sp. strain CBS-3. This enzyme catalyzes the hydrolysis of 4-chlorobenzoyl-CoA to 4-hydroxybenzoyl-CoA. The molecular structure of the enzyme/4-hydroxybenzoyl-CoA complex was solved by the techniques of multiple isomorphous replacement, solvent flattening, and molecular averaging. Least-squares refinement of the protein model reduced the crystallographic *R* factor to 18.8% for all measured X-ray data from 30 to 1.8 Å resolution. The crystallographic investigation of this dehalogenase revealed that the enzyme is a trimer. Each subunit of the trimer folds into two distinct motifs. The larger, N-terminal domain is characterized by 10 strands of β-pleated sheet that form two distinct layers which lie nearly perpendicular to one another. These layers of β-sheet are flanked on either side by α-helices. The C-terminal domain extends away from the body of the molecule and is composed of three amphiphilic α-helices. This smaller domain is primarily involved in trimerization. The two domains of the subunit are linked together by a cation, most likely a calcium ion. The 4-hydroxybenzoyl-CoA molecule adopts a curved conformation within the active site such that the 4-hydroxybenzoyl and the adenosine moieties are buried while the pantothenate and pyrophosphate groups of the coenzyme are more solvent exposed. From the three-dimensional structure it is clear that Asp 145 provides the side-chain carboxylate group that adds to form the Meisenheimer intermediate and His 90 serves as the general base in the subsequent hydrolysis step. Many of the structural principles derived from this investigation may be directly applicable to other related enzymes such as crotonase.

During the latter part of this century, synthetic chlorinated organic compounds have been released into the environment as a result of commercial production and careless waste disposal (Hileman, 1993). Biotoxicity, coupled with chemical stability, has rendered these compounds environmentally hazardous (Hooper *et al.,* 1990; Borlakoglu & Haegele, 1991). The potential for bioremediation using soil bacteria that have adapted through prolonged exposure to various target compounds offers exciting new promise (Abramowicz, 1990; Commandeur & Parsons, 1990; Higson, 1992; Slater *et al.,* 1995). Known as "environmentally directed evolution", this process of adaptation has taken center stage in the effort to engineer new biodegradative chemical pathways in prokaryotes. The 4-chlorobenzoate degrading pathway found in *Pseudomonas* sp. strain CBS-3 (Klages & Lingens, 1980) is a clear example of evolution directed by the availability of a new carbon source. The 4-chlorobenzoate operon consists of a regulatory site, under the positive control of 4-chlorobenzoate, and three structural genes encoding 4-chlorobenzoyl-CoA ligase, 4-chlorobenzoyl-CoA dehalogenase, and 4-hydroxybenzoyl-CoA thioesterase (Savard *et al.,* 1992). Proteins that share significant amino acid sequence identities with the 4-chlorobenzoate pathway enzymes have been recently identified (Babbitt *et al.,* 1992; Dunaway-Mariano & Babbitt, 1994). The focus of the present study, 4-chlorobenzoyl-CoA dehalogenase (Chang *et al.,* 1992; Löffler *et al.,* 1995; Crooks & Copley, 1994), is structurally related to both 2-enoyl-CoA hydratase (crotonase) and Δ^3-*cis*-Δ^2-*trans*-enoyl-CoA isomerase found in the fatty acid β-oxidation cycle, dihydroxynaphthoate synthase of the menaquinone pathway, and carnitine racemase of the carnitine pathway.

The 4-chlorobenzoyl-CoA dehalogenase is of particular interest in that it catalyzes a hydrolytic substitution reaction. Mechanistic studies of the dehalogenase have demonstrated a quite specialized mode of catalysis in which an active site carboxylate side chain is employed in the displacement of the chloride ion from the ring (Yang *et al.,* 1994). As indicated in Scheme 1, the arylated enzyme intermediate formed is hydrolyzed by attack of a water molecule at the acyl carbon, thereby avoiding the coupling of Meisenheimer complex formation and H_2O activation/addition into a single step.

[†] This research was supported in part by grants from the NIH (GM36260 to D.D.M. and DK47814 to H.M.H.).

[‡] Coordinates have been deposited in the Brookhaven Protein Data Bank under the identification code 1NZY.

* To whom correspondence should be addressed.

[§] University of Wisconsin.

[||] University of Maryland.

[⊗] Abstract published in *Advance ACS Abstracts,* June 1, 1996.

S0006-2960(96)00768-4 CCC: $12.00

Scheme 1

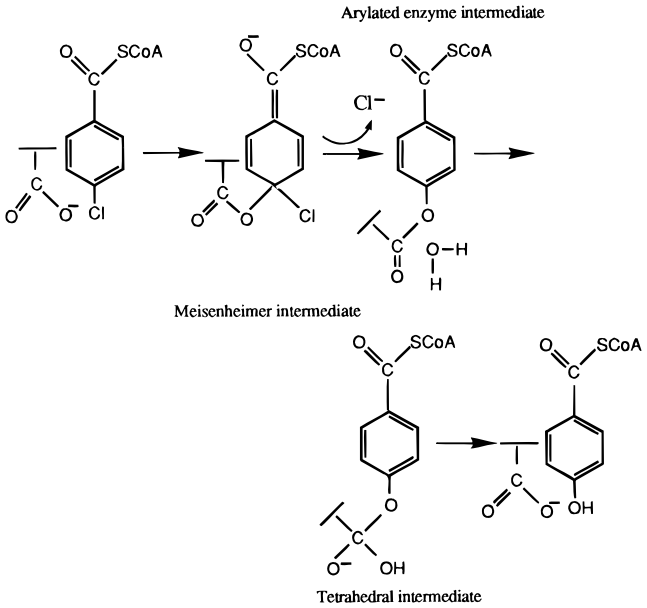

Spectral studies of various benzoyl-CoA adducts bound to the dehalogenase indicate significant redistributions of the π-electron densities in the conjugated C═C and C═O bonds of the ligands induced by the local protein environment (Taylor *et al.*, 1995). Electron withdrawal from the benzoyl-ring C(4) of the dehalogenase substrate through enzyme interaction with the thioester carbonyl would activate the substrate for nucleophilic attack and, thus, constitute "electrophilic catalysis" (Taylor *et al.*, 1995). Indeed, the rate-limiting step of the dehalogenation reaction is associated with the hydrolysis of the arylated intermediate and not with the nucleophilic aromatic substitution (Liu *et al.*, 1995).

Here we describe the three-dimensional structure of the 4-chlorobenzoyl-CoA dehalogenase complexed with 4-hydroxybenzoyl-CoA determined to a nominal resolution of 1.8 Å. The structure presented here provides the first detailed description of the active site geometry of this remarkable enzyme and yields new insights into its catalytic mechanism. Many of the general structural concepts derived from this study will be directly applicable to other related enzymes including crotonase.

MATERIALS AND METHODS

Crystallization and Preparation of Heavy Atom Derivatives. The enzyme employed in this investigation was purified according to a previously published procedure (Chang *et al.*, 1992), as modified in Taylor (1996). The structure of the H90Q mutant form of the enzyme was solved first since it crystallized more readily than the native enzyme. Thus it was possible to obtain the necessary supply of X-ray diffraction quality crystals for subsequent heavy atom derivative searches.

Large single crystals of the H90Q mutant protein complexed with 4-hydroxybenzoyl-CoA (Merkel *et al.*, 1989) were grown by batch methods and microseeding techniques from 8% poly(ethylene glycol) 8000, 200 mM potassium chloride, 50 mM CHES (pH 9.0), and 5 mM NaN_3 at 4 °C. Growth was generally complete within 1 week, with some crystals achieving dimensions of 0.7 mm × 0.5 mm × 0.3 mm. The protein and product concentrations were typically 400 μM and 2 mM, respectively. The same conditions were employed to crystallize the native enzyme complexed with 4-hydroxybenzoyl-CoA.

Both the H90Q mutant and the native protein crystals belonged to the space group $P2_12_12$ with unit cell dimensions of a = 107.8 Å, b = 102.4 Å, and c = 90.3 Å and three subunits per asymmetric unit. The solvent content of the crystals was approximately 54%. X-ray diffraction maxima were observed to at least 1.8 Å resolution for both protein crystal forms.

For heavy atom derivative searches, the H90Q mutant protein crystals were transferred to a synthetic mother liquor containing 12% poly(ethylene glycol) 8000, 50 mM CHES (pH 9.0), 200 mM KCl, and 5 mM NaN_3 and allowed to equilibrate overnight at 4 °C. Subsequently, the crystals were transferred to the same synthetic mother liquor except that the CHES buffer was replaced with 50 mM HEPES (pH 7.5). Following equilibration for 5 h, the crystals were transferred to another synthetic mother liquor containing 12% poly(ethylene glycol) 8000, 50 mM HEPES (pH 7.5), 200 mM KCl, 5 mM NaN_3, and 1 mM iodoacetamide and allowed to soak overnight. Following back-soaking for 5 h in a synthetic mother liquor lacking iodoacetamide, the crystals were then transferred to various heavy atom containing solutions. Four isomorphous heavy atom derivatives were prepared using 4 mM trimethyllead acetate, 2 mM potassium tetrachloroplatinate (II), 1 mM *p*-(hydroxymercuri)benzoate, and a saturated solution of ammonium hexabromoiridate-(IV). Without pretreatment of the crystals with iodoacetamide, most of the heavy atom compounds tested destroyed the crystalline lattice.

X-ray Data Collection and Processing. All X-ray data for the H90Q mutant protein and heavy atom derivative crystals were collected at 4 °C with a Siemens X1000D area detector system. The X-ray source was nickel-filtered Cu Kα radiation from a Rigaku RU200 X-ray generator operated at 50 kV and 90 mA and equipped with a 300 μm focal cup. Friedel pairs were measured for the platinum- and iridium-containing crystals. The H90Q native data set and the heavy atom derivative data sets were collected to 1.9 and 3.0 Å resolution, respectively.

All X-ray data from the H90Q mutant protein and the heavy atom derivatives were processed with the data reduction software package XDS (Kabsch, 1988a,b) and internally scaled according to a procedure developed in the laboratory by Dr. Gary Wesenberg. Relevant X-ray data collection statistics can be found in Table 1. Each heavy atom derivative X-ray data set was placed on the same scale as the native X-ray data set by a "local" scaling procedure developed by Drs. G. Wesenberg, W. Rypniewski, and I. Rayment. The R factors (based on amplitudes) between the native and the lead, platinum, mercury, and iridium data sets were 15.3%, 17.1%, 17.2%, and 13.8%, respectively.

X-ray data from a single native protein crystal complexed with product were collected at the Stanford Synchrotron Radiation Laboratory at −165 °C. Prior to freezing, the native crystal was transferred to a synthetic mother liquor containing 12% poly(ethylene glycol) 8000, 300 mM potassium chloride, 20% ethylene glycol, 50 mM CHES (pH 9.0), and 5 mM NaN_3. X-ray data collection statistics for the native crystal can be found in Table 1.

Structural Determination and Least-Squares Refinement. The positions of the heavy atom binding sites were deter-

Table 1: Intensity Statistics

resolution range (Å)	overall	30.0−6.00	4.76	4.16	3.78	3.51	3.30	3.14	3.00
H90Q									
completeness of data (%)	98	98	100	99	99	99	98	97	96
R factor (%)	2.2	1.6	1.9	1.9	2.2	2.5	2.8	3.4	4.0
potassium tetrachloroplatinate(II)									
completeness of data (%)	98	98	99	99	99	98	97	97	95
R factor (%)	3.9	3.1	3.5	3.3	3.8	4.9	5.8	7.5	10.0
ammonium hexabromoiridate(IV)									
completeness of data (%)	95	98	99	99	97	95	92	89	87
R factor (%)	2.3	1.7	1.8	1.7	2.2	2.7	3.6	4.6	6.0
p-(hydroxymercuri)benzoate									
completeness of data (%)	90	95	98	97	95	91	86	81	77
R factor (%)	4.8	2.5	3.8	3.9	5.1	6.7	8.9	12.2	16.2
trimethyllead acetate									
completeness of data (%)	88	91	93	92	91	89	87	85	74
R factor (%)	4.3	2.2	3.3	3.7	4.9	6.7	8.8	11.6	15.6

resolution range (Å)	overall	30.0−3.60	2.86	2.50	2.27	2.11	1.98	1.88	1.80
native									
completeness of data (%)	98	98	99	99	98	98	97	96	95
R factor (%)	3.6	3.4	4.0	4.1	3.5	3.8	4.6	5.7	6.6

[a] R factor $= (\sum|I - \bar{I}|/\sum I) \times 100$.

Table 2: Phase Calculation Statistics

	resolution range (Å)							
	∞−10.49	6.73	5.29	4.50	3.98	3.61	3.32	3.10
no. of reflections	1052	1787	2241	2623	2930	3206	3477	3476
figure of merit	0.69	0.70	0.65	0.59	0.56	0.53	0.51	0.48
phasing power[a]								
K_2PtCl_4								
centric reflections	1.06	1.24	1.19	1.06	0.92	0.99	1.12	1.00
acentric reflections	1.26	1.58	1.40	1.21	1.26	1.15	1.31	1.30
hexabromoiridate								
centric reflections	1.14	1.12	0.91	0.68	0.62	0.60	0.53	0.57
acentric reflections	1.53	1.48	1.21	0.94	0.90	0.87	0.81	0.85
p-(hydroxymercuri)benzoate								
centric reflections	1.22	1.27	0.94	0.93	0.98	0.96	1.03	0.95
acentric reflections	1.62	1.85	1.39	1.14	1.24	1.17	1.19	1.25
trimethyllead acetate								
centric reflections	0.88	0.93	0.89	0.67	0.65	0.59	0.62	0.60
acentric reflections	1.27	1.38	1.17	0.92	0.94	0.82	0.80	0.87

[a] Phasing power is the ratio of the root-mean-square heavy atom scattering factor amplitude to the root-mean-square lack of closure error.

mined by inspection of appropriate difference Patterson maps calculated to 5.0 Å resolution. The lead, platinum, mercury, and iridium derivatives contained 1, 3, 3, and 2 heavy atom binding sites, respectively. The derivatives were placed on a common origin by difference Fourier maps, and the positions and occupancies for each heavy atom binding site were refined by the origin-removed Patterson-function correlation method to 3.0 Å resolution (Rossmann, 1960; Terwilliger & Eisenberg, 1983). Anomalous difference Fourier maps were employed for determining the correct hand of the heavy atom constellation. Protein phases were calculated with the program HEAVY (Terwilliger & Eisenberg, 1983), and relevant phase calculation statistics can be found in Table 2.

An electron density map of the H90Q mutant protein, calculated to 3.0 Å resolution, clearly revealed the molecular boundaries of the three subunits in the asymmetric unit and many of the secondary structural elements. The electron density map was further improved by the techniques of solvent flattening and molecular averaging around the local 3-fold rotation axis at 3.0 Å resolution (Bricogne, 1976). A model for one subunit of the dehalogenase was constructed according to this "averaged" map with the program FRODO (Jones, 1985). The course of the polypeptide chain was unambiguous. Subsequently, the averaged subunit was placed back into the unit cell and the model subjected to alternate cycles of least-squares refinement with the program TNT (Tronrud *et al.*, 1987) and manual model building at 1.9 Å resolution.

The refined H90Q mutant structure served as the starting model for the refinement of the native enzyme structure to 1.8 Å resolution. Since the three-dimensional structures of the native and mutant enzymes are nearly identical, except in the immediate region surrounding the mutation, only the native structure will be described here. The final *R* factor for the native enzyme model was 18.8% with all measured X-ray data from 30 to 1.8 Å. The root-mean-square deviations from "ideal" geometry for the model were 0.015 Å for bond lengths, 2.31° for bond angles, and 0.008 Å for groups of atoms expected to be coplanar. The only amino acid residue missing from the model was Arg 257 in subunit III. This residue resides in a flexible loop. The final refined model includes 598 water molecules and 806 amino acid residues. The average temperature factor for the waters was 32.6 A^2. Three of these solvents refined to anomalously low *B* values. In addition, the octahedral geometry surrounding

FIGURE 1: Ribbon representations of the 4-chlorobenzoyl-CoA dehalogenase. These figures were prepared with the software package MOLSCRIPT (Kraulis, 1991). (a) Each subunit is displayed in a different color with the bound products, 4-hydroxybenzoyl-CoA, depicted in ball-and-stick representations. (b) Ribbon representation of one subunit of the dehalogenase. The position of the calcium ion connecting the two domains is indicated by the green sphere.

these putative waters suggested that they might be a cations, possibly calcium or sodium ions. When included in the model as calciums, they refined with temperature factors of 14.9, 16.4, and 28.9 Å^2, for subunits I, II, and III, respectively. In addition to the waters and calcium ions, two ethylene glycol molecules and one phosphate anion were also included in the model.

RESULTS

Tertiary and Quaternary Structure. Contrary to published reports regarding the tetrameric quaternary structure of 4-chlorobenzoyl-CoA dehalogenase (Chang *et al.*, 1992), the enzyme clearly packs as a trimer in the crystalline lattice with each of the three active sites separated by approximately 42 Å and related by a 3-fold rotational axis as shown in Figure 1a. The trimer can be described as a flattened sphere with overall dimensions of 45 Å × 86 Å × 79 Å. The surface area lost upon trimer formation is approximately 4600 Å^2, as calculated according to the method of Lee and Richards (1971) with a probe sphere of 1.4 Å. All backbone atoms for the three subunits constituting the trimer superimpose with a root-mean-square deviation of 0.36 Å. Since the three subunits of the trimer are overall very similar, the following discussion will refer only to subunit I unless otherwise indicated.

As displayed in Figure 1b, each subunit contains two distinct domains: a larger N-terminal or catalytic domain formed by Met 1 to Ala 205 and Val 263 to Val 269 and a smaller, entirely α-helical domain, delineated by Pro 206 to Gln 262. Nearly 78% of the polypeptide chain backbone atoms fold into classical secondary structural elements. The N-terminal domain is composed of eight α-helices which range in length from 3 to 24 residues and 10 strands of β-pleated sheet. These secondary structural elements are linked together by a variety of reverse turns including five type I, one type I′, one type II′, and one type III′. The 10 β-strands form two layers of mixed sheet which lie nearly at right angles to each other. A topological diagram of the N-terminal domain is shown in Figure 2. The first layer of sheet is composed of β-strands A, B, C, E, G, and J with the N-terminal strand running antiparallel and the remaining strands lying parallel. Likewise, the smaller β-sheet of the N-terminal domain is a mixture of three parallel β-strands, D, F, and H, and one antiparallel β-strand, I. As described

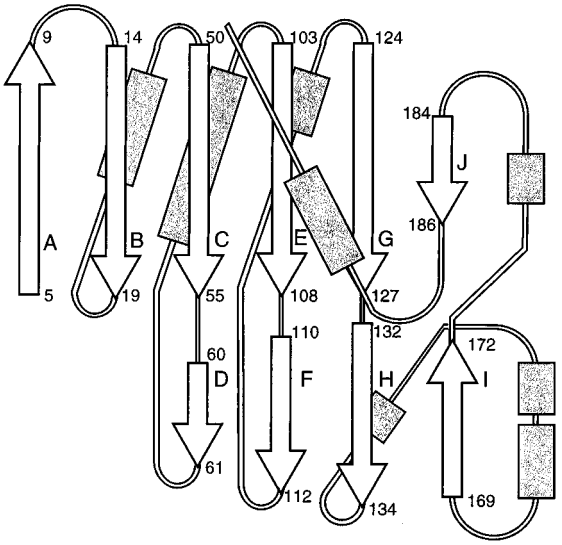

FIGURE 2: Topological diagram for the large domain of the dehalogenase subunit. β-Strands are represented as arrows while α-helices are displayed as cylinders. The numbering refers to those amino acid residues at the beginning and end of the β-strands.

below, those residues that lie within 3.8 Å of the 4-hydroxybenzoyl-CoA product reside either in random coil regions, in reverse turns, or in α-helices. The β-sheet motif of the N-terminal domain merely provides the scaffold for proper positioning of the active site amino acid residues.

While the dihedral angles for most of the amino acids lie within the allowed regions of the Ramachandran plot, Glu 57 adopts ϕ,ψ angles of 56.1° and −130.0°, respectively. This type of unfavorable interaction has been observed in various hydrolytic enzymes containing the α/β hydrolase fold (Ollis *et al.*, 1992). In these enzymes, it is the nucleophile of the so-called "catalytic triad" that adopts strained ϕ,ψ angles and resides in a γ-like turn linking a β-strand and an α-helix. In the 4-chlorobenzoyl-CoA dehalogenase, Glu 57 is located in a type II′ turn positioned between β-strands C and D and is followed in amino acid sequence by an aspartate. Glu 57 is approximately 13 Å from the active site and as such most likely does not play a role in the catalytic mechanism. Interestingly, these strained dihedral angles have also been observed for Glu 159 in phosphotriesterase, another enzyme that has attracted recent attention as a possible bioremediation agent (Benning *et al.*, 1994, 1995). As in the 4-chlorobenzoyl-CoA dehalogenase, Glu 159 resides in a type II′ turn and is followed by an aspartate. The functional significance of these strained dihedral angles in 4-chlorobenzoyl-CoA dehalogenase and phosphotriesterase is presently not understood.

The C-terminal domain of the 4-chlorobenzoyl-CoA dehalogenase structure extends away from the body of the molecule and is composed of three amphiphilic α-helices. This smaller domain is primarily involved in trimerization. Subunit/subunit interactions are substantially hydrophobic with only one buried glutamate residue, Glu 232. There are three tryptophans, each contributed by one subunit (Trp 221), that form a crown at the top of the trimer as indicated in Figure 1a. In addition to stacking interactions, these tryptophans are further linked together by hydrogen bonds between their carbonyl oxygens and side-chain nitrogens. As shown in Figure 1b, the connecting α-helices between the catalytic and trimerization domains, delineated by Phe 191 to Ala 204 and Thr 207 to Ala 219, are stabilized by the presence of a cation, most likely a calcium ion. The calcium is surrounded in an octahedral environment by four ligands provided by carbonyl oxygens (Gly 49, Leu 202, Ala 203, Ala 205) and two contributed by amino acid side chains (O^{γ} of Thr 207 and $O^{\epsilon 1}$ of Gln 210). Bonds between the calcium ion and the oxygen ligands range in length from 2.6 to 2.8 Å.

Active Site Geometry. Electron density corresponding to the 4-hydroxybenzoyl-CoA moiety is displayed in Figure 3. As can be seen, the ligand adopts a closed conformation such that the amide nitrogen of the pantothenate unit lies within 3.1 Å of N7 of the adenine ring. The ribose ring is in the $C_{2'}$-endo configuration. There is no electron density for the 3′-phosphate group of the CoA ribose in each of the three molecules in the asymmetric unit. The lack of the phosphate moiety suggests that either hydrolysis occurred during the crystallization experiments or the original ligand solutions employed in the investigation were contaminated with a minor population of CoA molecules lacking 3′-phosphate groups. Experiments are presently underway to distinguish between these two possibilities. Note that, due to crystal packing constraints, it is not possible to accommodate a 3′-phosphate group on the CoA molecule in subunit I of the

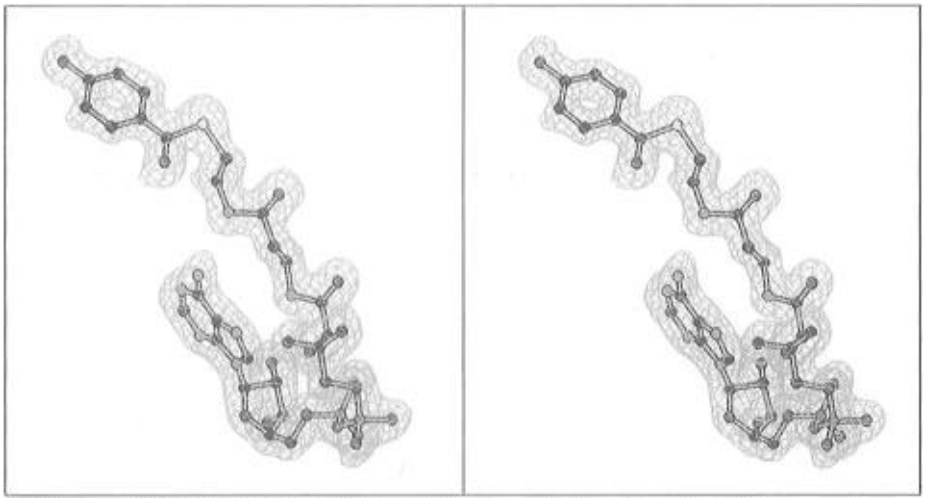

FIGURE 3: Representative electron density. Electron density corresponding to the bound product is shown. The electron density displayed was calculated to 1.8 Å resolution with coefficients of the form $(2F_o - F_c)$, where F_o and F_c were the native and calculated structure factor amplitudes, respectively. The map was contoured at 1σ.

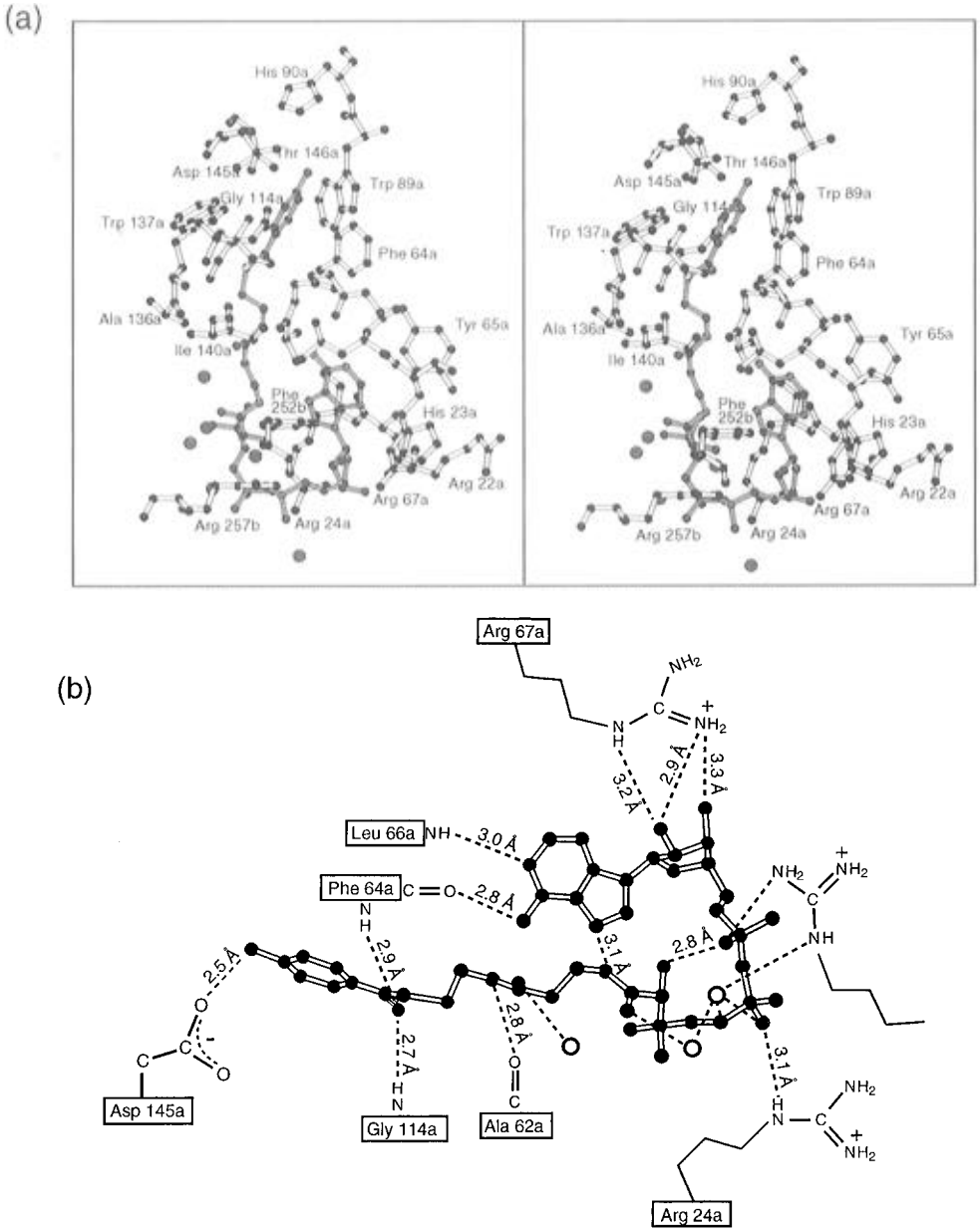

FIGURE 4: Structural features of the active site of the dehalogenase. (a) Close-up view of the active site for subunit I is displayed with those amino acid residues located within approximately 3.8 Å of the 4-hydroxybenzoyl-CoA product. (b) Schematic representation of the electrostatic interactions between the protein and the product in subunit I are indicated by the dashed lines. Those residues with the suffix "b" are contributed by subunit II in the trimer. The bond lengths indicated are average values observed for the three subunits constituting the trimer. Due to crystal packing, the protein/product interactions in the vicinity of the pantothenate and pyrophosphate moieties are slightly different in subunits II and III. Water molecules are indicated by the open circles.

trimer although subunits II and III could bind a phosphorylated nucleotide. There is a positively charged pocket formed by His 23 and Arg 67 which most likely interacts with the 3′-phosphate group of the intact nucleotide.

The active site, as depicted in Figure 4a, is formed by two subunits. Most of the amino acids constituting the active site are provided by one subunit, but several amino acid residues, including Phe 252 and Arg 257, are contributed by a neighboring molecule in the trimer. The environment surrounding the 4-hydroxybenzoyl moiety of the product is decidedly hydrophobic. There are three residues, Phe 64, Trp 89, and Trp 137, that form a ring around the bound ligand and participate in perpendicular stacking interactions with its 4-hydroxybenzoyl moiety. Most of the specific interactions between the ligand and the protein occur through backbone amide nitrogens and carbonyl oxygens. A cartoon of potential hydrogen bonds between the protein and the product is given in Figure 4b. While the 4-hydroxybenzoyl and adenosine portions of the product are buried, both the pantothenate unit and the pyrophosphate moiety are more solvent exposed. There are two specific electrostatic interactions between the product and the protein in this region. The first occurs between the guanidinium group of Arg 24 and the phosphate group immediately following the pantothenate unit of the coenzyme. The second phosphate group, as shown in Figure 4b, interacts with the side chain of Arg 257 from a neighboring subunit. The adenine ribose is anchored to the protein through the guanidinium group of Arg 67. The most striking interaction between the 4-hydroxybenzoyl-CoA ligand and the protein occurs via Asp 145. One of the carboxylate side-chain oxygens of Asp 145 lies within 2.5

Å of the 4-hydroxyl group and 3.0 Å of the C(4) of the benzoate ring.

DISCUSSION

From the three-dimensional model of the 4-chlorobenzoyl-CoA dehalogenase presented here, it is now possible to understand its catalytic mechanism in structural terms. As shown in Scheme 1, the first step of the reaction catalyzed by the enzyme involves attack of a carboxylate side chain on C(4) of the benzoate ring (Yang *et al.*, 1994; Liu *et al.*, 1995). From this investigation it is now obvious that the carboxylate side chain necessary for catalysis is provided by Asp 145. Indeed, a site-directed mutant in which Asp 145 has been replaced by an alanine is catalytically inactive (G. Yang, R.-Q. Liu, K. L. Taylor, H. Xiang, J. Price, and D. Dunaway-Mariano, manuscript in preparation). As indicated in Figure 4b, the thioester carbonyl of the ligand is within hydrogen-bonding distance of the backbone amide hydrogen atoms of Gly 114 and Phe 64. In addition, Gly 114 is positioned at the N-terminal end of the α-helix delineated by Gly 114 to Ala 121. Complexation of the substrate ligand results in significant changes in the benzoyl C═O and ring C═CH Raman bands and in a shift of the benzoyl absorption maximum from 260 to 302 nm (Taylor *et al.*, 1995). Recent spectral studies of dehalogenase mutants (Liu *et al.*, 1996) implicate the helix dipole as the cause of the redistribution of ring π-electron density. It can thus be speculated that polarization of the thioester carbonyl through interaction with the positive end of this helix dipole activates the benzoyl ring C(4) toward nucleophilic attack by Asp 145 and stabilizes the resulting Meisenheimer intermediate.

The second step of the dehalogenase reaction is the hydrolysis of the arylated Asp 145. This reaction occurs by addition of a water molecule at the acyl carbon with displacement of the phenol(ate). On the basis of the current three-dimensional model of the dehalogenase/product complex, it can be speculated that the acyl carbonyl oxygen atom of the arylated intermediate lies within hydrogen-bonding distance to $N^{\epsilon 1}$ of Trp 137. As such, this electrostatic interaction might serve to position the carbonyl carbon for nucleophilic attack and subsequently to stabilize the resulting oxyanion. His 90 appears to be the only base within the general vicinity of the active site that could activate the attacking water molecule. In addition, as the conjugate acid, His 90 might serve to reprotonate the phenoxide oxygen which, in the ensuing step, dissociates from the tetrahedral intermediate. In support of this argument it should be noted that the H90Q mutant forms the Meisenheimer complex readily ($k = 67\ s^{-1}$), but the rate of product formation is quite slow ($k = 0.0009\ s^{-1}$) (Liu and Dunaway-Mariano, unpublished results). While the active site of the crystalline enzyme/4-hydroxybenzoyl-CoA complex does not contain a water molecule, it might be speculated that, in the arylated enzyme intermediate, a water molecule would be positioned between His 90 and Asp 145. Although the molecular architecture of the dehalogenase presented here appears to be unlike that of any other known protein structure, a significant level of amino acid sequence identity exists between it and 2-enoyl-CoA hydratase (crotonase), Δ^3-*cis*-Δ^2-*trans*-enoyl-CoA isomerase, dihydroxynaphthoate synthase, and carnitine racemase (30% identity, 60% similarity). Most likely, these enzymes will also have similar structural motifs. Indeed, the residues of the active site α-helix (Gly 114 to Ala 121) that is positioned for polarization of the substrate benzoyl C═O are highly conserved in these proteins. As with the dehalogenase, each of these enzymes carries out catalysis via an enolate thioester intermediate and/or a transition state requiring stabilization through interaction with an electropositive active site group [see Dunaway-Mariano and Babbitt (1994)].

ACKNOWLEDGMENT

We thank Dr. W. W. Cleland for critically reading the manuscript and Dr. Ivan Rayment for preparing Figure 2.

REFERENCES

Abramowicz, D. A. (1990) *Crit. Rev. Biotechnol. 10*, 241−251.
Babbitt, P. C., Kenyon, G. L., Martin, B. M., Charest, H., Sylvestre, M., Scholten, J. D., Chang, K.-H., Liang, P.-H., & Dunaway-Mariano, D. (1992) *Biochemistry 31*, 5594−5604.
Benning, M. M., Kuo, J. M., Raushel, F. M., & Holden, H. M. (1994) *Biochemistry 33*, 15001−15007.
Benning, M. M., Kuo, J. M., Raushel, F. M., & Holden, H. M. (1995) *Biochemistry 34*, 7973−7978.
Borlakoglu, J. T., & Haegele, K. D. (1991) *Comp. Biochem. Physiol. 100C*, 327−338.
Bricogne, G. (1976) *Acta Crystallogr., Sect. A 32*, 832−847.
Chang, K.-H., Liang, P.-H., Beck, W., Scholten, J. D., & Dunaway-Mariano, D. (1992) *Biochemistry 31*, 5605−5610.
Commandeur, L. C., & Parsons, R. J. (1990) *Biodegradation 1*, 207−220.
Crooks, G. P., & Copley, S. D. (1994) *Biochemistry 33*, 11645−11649.
Dunaway-Mariano, D., & Babbitt, P. C. (1994) *Biodegradation 5*, 259−276.
Higson, F. K. (1992) *Adv. Appl. Microbiol. 37*, 135−164.
Hileman, B. C. (1993) *Chem. Eng. News 71*, 11−20.
Hooper, S. W., Pettigrew, C. A., & Sayler, G. S. (1990) *Environ. Toxicol. Chem. 9*, 655−667.
Jones, T. A. (1985) *Methods Enzymol. 115*, 157−171.
Kabsch, W. (1988a) *J. Appl. Crystallogr. 21*, 67−71.
Kabsch, W. (1988b) *J. Appl. Crystallogr. 21*, 916−924.
Klages, U., & Lingens, F. (1980) *Zentralbl. Bakteriol., Parasitenkd., Infektionskrankh. Hgy., Abt. 1: Orig. C1*, 215.
Kraulis, P. J. (1991) *J. Appl. Crystallogr. 24*, 946−950.
Lee, B., & Richards, F. M. (1971) *J. Mol. Biol. 55*, 379−400.
Liu, R.-Q., Liang, P.-H., Scholten, J., & Dunaway-Mariano, D. (1995) *J. Am. Chem. Soc. 117*, 5003−5004.
Löffler, F., Lingens, F., & Muller, R. (1995) *Biodegradation 6*, 203−212.
Merkel, S. M., Eberhard, A. E., Gibson, J., & Harwood, C. S. (1989) *J. Bacteriol. 171*, 1−7.
Ollis, D. L., Cheah, E., Cygler, M., Dijkstra, B., Frolow, F., Franken, S. M., Harel, M., Remington, S. J., Silman, I., Schrag, J., Sussman, J. L., Verschueren, K. H. G., & Goldman, A. (1992) *Protein Eng. 5*, 197−211.
Rossmann, M. G. (1960) *Acta Crystallogr. 13*, 221−226.
Savard, P., Charest, H., Sylvestre, M., Shareck, F., Scholten, J. D., & Dunaway-Mariano, D. (1992) *Can. J. Microbiol. 38*, 1074−1083.
Slater, J. H., Bull, A. T., & Hardman, D. J. (1995) *J. Biodegrad. 6*, 181−189.
Taylor, K. L. (1996) Ph.D. Thesis, University of Maryland, College Park, MD.
Taylor, K. L., Liu, R.-Q., Liang, P.-H., Price, J., Dunaway-Mariano, D., Tonge, P. J., Clarkson, J., & Carey, P. R. (1995) *Biochemistry 34*, 13881−13888.
Terwilliger, T. C., & Eisenberg, D. (1983) *Acta Crystallogr., Sect. A 39*, 813−817.
Tronrud, D. E., Ten Eyck, L. F., & Matthews, B. W. (1987) *Acta Crystallogr., Sect. A 43*, 489−501.
Yang, G., Liang, P.-H., & Dunaway-Mariano, D. (1994) *Biochemistry 33*, 8527−8531.

BI960768P